# Capillary Evaporation in Pores

**R Roth†‡and K M Kroll†‡**

† Max-Planck Institut für Metallforschung, Heisenbergstraße 3, D-70589 Stuttgart, Germany
‡ Institut für Theoretische und Angewandte Physik, Universität Stuttgart, Pfaffenwaldring 57, D-70569 Stuttgart, Germany

E-mail: Roland.Roth@mf.mpg.de

**Abstract.** We combine a density functional theory (DFT) treatment of capillary evaporation in a cylindrical pore with the morphometric approach in order to study the formation and breaking of bubbles in a hydrophobically lined part of a cone. The morphometric approach, in which the grand potential of a system is described in four geometrical terms with corresponding thermodynamical coefficients, allows extrapolation or scaling from macroscopic system sizes to nanoscales. Since only a small number of fluid particles are involved in bubble formation, it is a pseudo phase transition, and the system is subjected to strong fluctuations between states with and without a bubble. Fluctuations are not included in a DFT treatment, which makes it possible to explore both states of the system in great detail, in contrast to computer simulations, in which averages might be obscured by fluctuations.

## 1. Introduction

The physics of confined fluids has been studied in great detail both experimentally [1–7] and theoretically [8–12]. Several phenomena are known to be produced by the confining geometry. For example, one finds that a fluid that is in the gas phase in bulk, i.e. without confinement, can condense into a liquid phase at a much higher density if confined by hydrophilic walls, despite the fact that this liquid would not be stable in the bulk. This phenomenon is called capillary condensation and can be observed in experiments measuring adsorption isotherms of gases in porous media. A closely related phenomenon is the transition of a fluid, in its stable bulk liquid phase, confined by hydrophobic walls, into a gas phase at much smaller number density, that would not be stable without the confining geometry. This transition is called capillary evaporation, or "bubble formation" in more colorful language. Both transitions show hysteresis loops [13] in experiments,which are typical signs for first order phase transitions.

Most of the experimental and theoretical effort was targeted at understanding these transitions in the case of fluids close to saturation. Theoretical studies often employed a simple slit geometry of two parallel planar walls. Under these conditions the transition can take place at a moderate level of confinement so that mesoscopic arguments based on thermodynamics have proven very helpful.

Recent studies indicate that a phenomenon similar to capillary evaporation might be important in the physics of ion channels [14–23]. Ion channels are proteins in cell membranes

that allow the passive transport of ions along their electro-chemical gradient [24]. The main function of these proteins is to control the transport of ions through the membrane by opening and closing the channel, a process called gating, and in some cases by allowing only specific ions to pass through the pore, a phenomenon called selectivity. Our work is inspired by the wish to improve the understanding of the role of bubble formation and breaking in the gating mechanism of ion channels.

To this end we start in Sec. 2 by recalling the basics of capillary evaporation in simple geometries using a thermodynamics point of view. Then we show in Sec. 3 microscopic density functional theory (DFT) calculations [25] of a square-well fluid inside an infinitely long hydrophobically lined cylinder. In our DFT calculations we focus on the density profile $\rho(r)$ and the corresponding grand potential $\Omega$ of a fluid as a function of the cylinder radius $R_{cyl}$ while capillary evaporation takes place. The insight gained from these DFT calculations we transfer to and exploit in our morphometric approach [26, 27], presented in Sec. 4. In morphometry the free energy of a liquid confined in a pore is expressed by four terms that describe the geometry of the pore and corresponding thermodynamic coefficients. This separation of geometry and thermodynamics allows us to extrapolate or scale the behavior of the system from macroscopic sizes down small sizes in the nanometer regime and below. Furthermore, the morphometric approach makes calculations very efficient so that the formation of a bubble in the gate due to a change in geometry can be studied in detail. The bubble formation in the geometry we consider constitutes a pseudo phase transition, in which a finite number of particles is involved. This makes the system close to the transition point unstable in the sense that thermal fluctuation can cause the formation or breaking of the bubble and the system will constantly change state. This varying behavior makes the bubble formation hard to study reproduceable and hence convincingly in computer simulations. We conclude with an outlook in Sec. 5.

## 2. Capillary Evaporation in Simple Geometries

We consider a square-well fluid in the grand canonical ensemble and describe its structure and thermodynamic properties within the framework of density-functional theory (DFT). The inter-particle interaction potential is given by

$$V_{sw}(r) = \begin{cases} \infty & r < 2R_{HS}, \\ -\varepsilon & 2R_{HS} \leq r < 2R_{sw}, \\ 0 & \text{otherwise}, \end{cases} \tag{1}$$

where $R_{HS}$ and $R_{sw}$ is the hard-sphere and the square-well radius, respectively, and $\varepsilon$ is the square-well depth. The functional $\Omega[\rho(\mathbf{r})]$ of the grand potential has the form [25]

$$\Omega[\rho(\mathbf{r})] = \mathcal{F}_{id}[\rho(\mathbf{r})] + \mathcal{F}_{ex}[\rho(\mathbf{r})] + \int d^3r\, \rho(\mathbf{r})\left(V_{ext}(\mathbf{r}) - \mu\right). \tag{2}$$

The intrinsic Helmholtz free energy functional $\mathcal{F}[\rho(\mathbf{r})] = \mathcal{F}_{id}[\rho(\mathbf{r})] + \mathcal{F}_{ex}[\rho(\mathbf{r})]$ can be split into an exactly known ideal gas contribution $\mathcal{F}_{id}[\rho(\mathbf{r})]$ and an approximate excess (over the ideal gas) free energy functional $\mathcal{F}_{ex}[\rho(\mathbf{r})] = \mathcal{F}_{ex}^{HS}[\rho(\mathbf{r})] + \mathcal{F}_{ex}^{sw}[\rho(\mathbf{r})]$. $V_{ext}(\mathbf{r})$ denotes the

external and $\mu$ the chemical potential of the fluid. $\mathcal{F}_{ex}[\rho(\mathbf{r})]$ can be further split into a hard-sphere reference part $\mathcal{F}_{ex}^{HS}[\rho(\mathbf{r})]$, for which we employ the White Bear version [28, 29] of fundamental measure theory [30], and a square-well part

$$\mathcal{F}_{ex}^{sw}[\rho(\mathbf{r})] = \frac{1}{2}\int d^3r' \int d^3r'' \rho(\mathbf{r}')\rho(\mathbf{r}'')V_{attr}(|\mathbf{r}' - \mathbf{r}''|), \tag{3}$$

with a simple mean-field approximation for the inter-particle attraction $V_{attr}(r)$, which is $-\varepsilon$ for $r < 2R_{sw}$ and zero otherwise. Except for the external potential $V_{ext}(\mathbf{r})$, which plays an important role in the present study of confined fluids, the system is fully specified.

Before considering confined fluids, we recall the bulk phase behavior of the square-well fluid. Since we are interested in fluid behavior, we assume that the density profile $\rho(\mathbf{r})$ reduces to the constant bulk density $\rho$. From the bulk grand potential $\Omega_{bulk} = \Omega[\rho(\mathbf{r}) = \rho]$ we calculate the bulk pressure $p(\rho) = -\Omega_{bulk}/V$, where $V$ is the volume, and the chemical potential $\mu(\rho) = \partial f/\partial\rho$, with the free energy density $f = F/V$. Two fluid phases, denoted by $I$ and $II$, with corresponding number densities $\rho_I$ and $\rho_{II}$ coexist when they are in mechanical and chemical equilibrium, i.e. if

$$p(\rho_I) = p(\rho_{II}), \quad \text{and} \quad \mu(\rho_I) = \mu(\rho_{II}). \tag{4}$$

For a square-well radius $R_{sw} = 3R_{HS}$ we obtain the fluid phase diagram shown in Fig. 1. Below the critical temperature, the fluid phase can separate into a liquid phase with a high bulk density and a gas phase with a low bulk density. Note that the mean-field perturbation theory, Eq. (3), predicts a phase diagram that is not sensitive to the detailed choice of parameters $\varepsilon$ and $R_{sw}$. It rather predicts phase diagrams that can be rescaled onto a 'master phase diagram'. One finds, using the Carnahan-Starling equation of state for the hard-sphere contribution, that the critical point is located at $\eta_c \approx 0.1304$ and $k_BT_c/\varepsilon \approx 0.0472(R_{sw}/R_{HS})^3$.

If we bring a square-well liquid in contact with a single purely repulsive planar wall, the fluid develops, in general, an inhomogeneous density profile $\rho(z)$, where $z$ denotes the distance from the wall. $\rho(z)$ can be calculated by minimizing the DFT [25] with an appropriate external wall potential that accounts for the interaction between the liquid and a hydrophobically lined pore. For a liquid state very close to the coexisting density $\rho_{II}(T)$ one can observe complete drying [31] and a growth of a macroscopically thick gas film at the wall as the density $\rho$ approaches the coexisting liquid density $\rho_{II}$ at a given temperature $T$, or as the deviation $\delta\mu = \mu - \mu_{co}(T)$ of the chemical potential from its value at coexistence $\mu_{co}(T)$ approaches zero.

In the present study, however, we shall stay away from these state points, as indicated in the phase digram in Fig. 1 by the state with reduced temperature $k_BT/\varepsilon = 0.9174$ and packing fraction $\eta = 4\pi R_{HS}^3\,\rho/3 = 0.3842$.

In order to quantify the change in the grand potential due to the inhomogeneous structure $\rho(z)$ close to the wall we define $\sigma$, the planar wall surface tension as

$$\sigma = \frac{1}{A}\left(\Omega[\rho(z)] + pV\right), \tag{5}$$

by subtracting the bulk term $-pV$ from the total grand potential of the system $\Omega = \Omega[\rho(z)]$. $A$ is the surface area of the wall. In the thermodynamical limit, $V \to \infty$, the grand potential

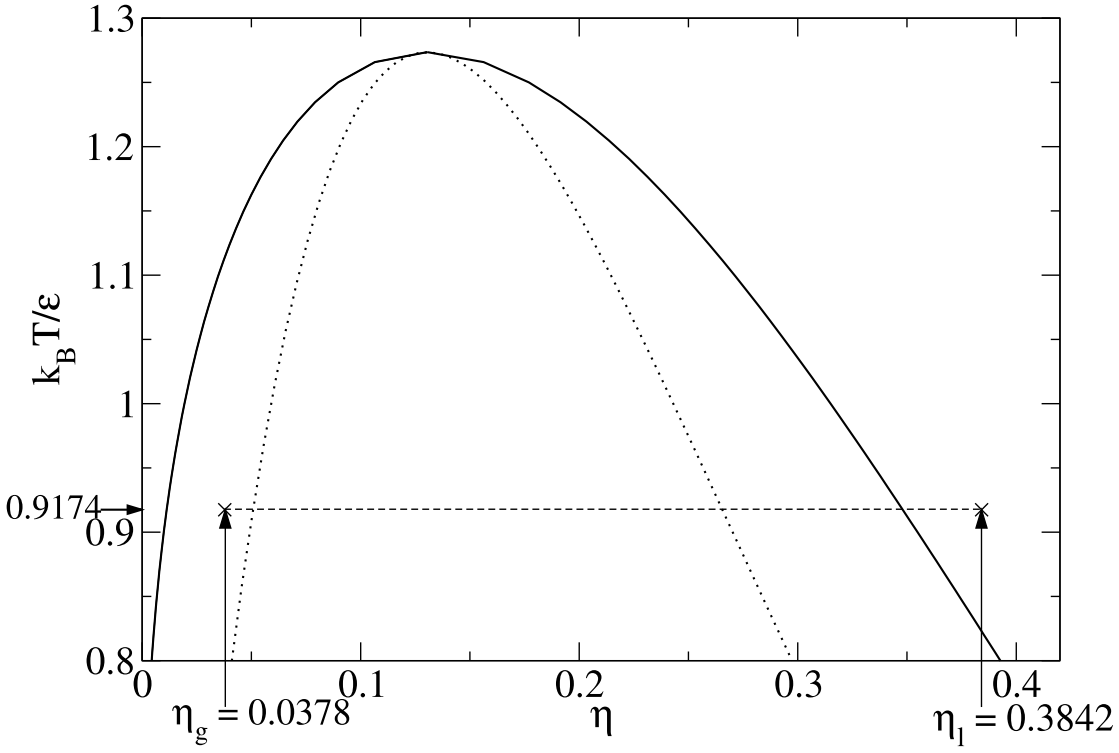


**Figure 1.** The fluid-gas binodal of a square-well fluid with $R_{sw} = 3R_{HS}$ as function of reduced temperature $k_BT/\varepsilon$ and the fluid packing fraction $\eta = 4\pi R_{HS}^3\ \rho/3$. In our DFT calculation we consider the reduced temperature $k_BT/\varepsilon = 0.9174$ and a fluid packing fraction of $\eta_l = 0.3842$. We find that a gas with $\eta_g = 0.0378$ has the same chemical potential as the corresponding liquid.

$\Omega$ and $A$ also go to infinity. However, $\sigma$ is an intrinsic quantity and remains finite. Note that the value of $\sigma$ depends on the definition of the dividing surface [32] which in turn defines the volume $V$. However, the value of $\Omega = -pV + \sigma A$ remains the same for all definitions.

For a state point significantly far away from the binodal, as chosen in the present case, the interaction of the liquid and a single hydrophobic wall is not sufficient to destabilize the high density liquid in favor of a low density gas. The pressure in the liquid phase away from coexistence is always higher than in a gas phase at the same chemical potential so that the surface contribution to the grand potential cannot compete with the volume term. For the gas phase to be more stable than the liquid phase, its grand potential $\Omega_g = -p_gV + \sigma_gA$ must be more negative than the grand potential of the liquid phase $\Omega_l = -p_lV + \sigma_lA$, with $V = AL$ and $A, L \to \infty$ in the thermodynamic limit. This cannot be accomplished since even the smallest difference in the pressure would make the difference of the volume terms, $(-p_l + p_g)AL$, arbitrarily larger than the difference in the surface terms, $(\sigma_g - \sigma_l)A$.

When we add a second, parallel, wall at distance $L$ the behavior of the system changes *qualitatively*. We consider the situation of two identical walls for simplicity. Note, that the value of $L$ also depends on the definition of the dividing surface, i.e. it measures the distance between the parallel dividing surfaces of the opposing walls. If $L$ is large compared to the bulk correlation length $\xi$ of the liquid, the grand potential of the system in the slit geometry

can be written as [11]

$$\Omega_i^{slit} \approx -p_i V + 2\sigma_i A, \quad i = l, g, \tag{6}$$

where we have used that the walls are independent and the surface tensions $\sigma_i$ are those of a single wall. Since the volume term is now scaled by a finite length $L$, it is possible that the liquid phase is destabilized in a slit geometry for sufficiently small plate separations. For phase equilibrium between a liquid and a gas phase with densities $\rho_l$ and $\rho_g$, respectively, at a wall separation $L_{CE}$ it is necessary that their grand potentials and their chemical potentials are equal, which can be expressed, after dividing $\Omega_i^{slit}$ by the area $A$, as

$$-p_l L_{CE} + 2\sigma_l = -p_g L_{CE} + 2\sigma_g, \quad \text{and} \quad \mu(\rho_l) = \mu(\rho_g). \tag{7}$$

This equilibrium condition can be solved to determine the slit width

$$L_{CE} = \frac{2(\sigma_g - \sigma_l)}{p_g - p_l}, \tag{8}$$

at which the capillary evaporation (CE) transition takes place. Clearly, since $(p_g - p_l)$ is negative, Eq. (8) has a physical solution only if $(\sigma_g - \sigma_l)$ is also negative, which holds true for hydrophobic walls. Equation (7) or (8) describe a competition between the volume and the surface contributions to the grand potential of the two fluid phases.

For a slit width $L > L_{CE}$ the volume term in the grand potential dominates and stabilizes the liquid phase, whereas for $L < L_{CE}$ the surface term in the grand potential becomes more important and favors the gas phase. Note, that a gas that is stabilized in the slit pore has the same chemical potential as the liquid phase and would be meta-stable in the bulk, i.e. would lie between the binodal (full line) and spinodal (dotted line) at $\eta_g = 0.0378$ – see Fig. 1.

Before we switch to a more complicated geometry, it is very instructive to consider the phenomena of capillary evaporation in an infinitely long cylindrical pore. The (approximate) form of the grand potential in the slit pore, Eq. (6), is well known and tested, at least for state points close to saturation, against microscopic theories, but the case of a cylindrical pore seems less understood.

Following the morphometric approach, we propose that the grand potential in contact with a complexly shaped wall can be written as [26, 27]

$$\Omega_i \approx -p_i V + \sigma_i A + \kappa_i C + \bar{\kappa}_i X, \tag{9}$$

where $V$ and $A$ are, as before, the volume and surface area defined by the dividing interface. The corresponding thermodynamic coefficients are $-p_i$ and $\sigma_i$, the negative of the pressure and the *planar* wall surface tension in phase $i$, respectively. Two additional geometrical measures are required in order to take the effects of curvature of the dividing interface into account, namely

$$C \equiv \int_{\partial V} H dA, \quad \text{and,} \quad X \equiv \int_{\partial V} K dA \tag{10}$$

the integrated (over the surface area $A$) mean and Gaussian curvatures $H = (1/R_I + 1/R_{II})/2$ and $K = 1/(R_I R_{II})$, respectively. $R_I$ and $R_{II}$ are the two principal radii of curvature, which are positive if the curvature is convex and negative in the case of concave curvature.

The corresponding thermodynamic coefficients are the bending regities $\kappa_i$ and $\bar{\kappa}_i$. The morphometric form of the grand potential has been suggested to describe the thermodynamics of a fluid in contact with *convex* walls. However, away from a critical point or a wetting or drying transition the morphometric form of the grand potential should provide a good description also for a fluid inside of a pore, if the size of the pore is sufficiently large compared to the correlation length $\xi$. We will comment on this point, when we present our DFT results in the next section.

For an infinitely long cylinder with radius $R$, the geometrical measures are readily calculated and we obtain $V = R^2\pi L$, $A = 2\pi RL$ and $C = -\pi L$. Note that the integrated mean curvature $C$ is negative because we are considering the *inside* of the cylinder, where the curvature is concave and the radius of curvature negative. The fourth measure $X$ vanishes because the Gaussian curvature $K$ of a cylinder is always zero. Hence the morphometric form of the grand potential of a fluid inside a cylinder is given by,

$$\Omega_i^{cyl} \approx -p_i R^2\pi L + \sigma_i 2\pi RL - \kappa_i \pi L, \tag{11}$$

and we take the length of the cylinder $L \to \infty$. Using the morphometric form for $\Omega_i^{cyl}/(\pi L)$, we can formulate the equilibrium condition between a liquid and a gas phase inside of the cylindrical pore

$$-p_l R_{CE}^2 + 2\sigma_l R_{CE} - \kappa_l = -p_g R_{CE}^2 + 2\sigma_g R_{CE} - \kappa_g, \quad \text{and} \quad \mu(\rho_l) = \mu(\rho_g). \tag{12}$$

The radius $R_{CE}$ at which capillary evaporation takes place can be expressed explicitly in terms of the thermodynamic coefficients as

$$R_{CE} = \frac{(\sigma_g - \sigma_l) - \sqrt{((p_g - p_l)\ (\kappa_l - \kappa_g)) + (\sigma_g - \sigma_l)^2}}{p_g - p_l}. \tag{13}$$

It would be possible to proceed with a spherical cavity, however, the expression for the radius at which capillary evaporation takes place is rather lengthy and provides no additional insight.

## 3. DFT Treatment of Capillary Evaporation in Cylindrical Pores

In order to verify the validity of the morphometric approach for the description of capillary evaporation inside infinitely long cylindrical pores, we perform DFT calculations. We have to choose an external potential $V_{ext}(r)$ that defines the cylindrical pore. Since we wish to make a connection to the gating process in ion channels, we follow the approach from Ref. [33] and use a hard-sphere fluid of a given high density ($\eta_w = 0.4$, $R_w = 0.825R_{HS}$) which is kept outside of the pore region by a hard-wall potential. The square-well fluid inside the pore can hardly penetrate into the region which is occupied by the wall fluid. The wall fluid thereby exerts an effective external potential $V_{ext}(r)$ on the fluid inside the pore. We have calculated the external potential $V_{ext}(r)$ so that it leads to the same density profile $\rho(r)$ of the square-well fluid inside the pore as the wall fluid does. $V_{ext}(r)$ therefore corresponds to an atomically rough hydrophobic protein wall, which is averaged over the symmetry angle and the $z$-axes.

We perform a series of DFT calculation of a square-well fluid inside a cylindrical pore with radius $R_{cyl}$. We fix the reduced temperature $k_BT/\varepsilon = 0.9174$ and the chemical potential

so that it corresponds to a *bulk* packing fraction of the fluid $\eta = 0.3842$. The fluid density corresponds to a bulk concentration of 55.5M, the concentration of water at normal condition, if we assume that the hard-sphere radius $R_{HS} = 1.4\text{Å}$. This state point is considerably far from the binodal, that one can expect that a capillary evaporation transition will take place at rather small values of $R_{cyl}/R_{HS}$.

In Fig. 2 we show the equilibrium density profiles $\rho(r)$ for varying values of $R_{cyl}$. For $R_{cyl} \geq 6R_{HS}$ we find that the liquid phase is stable in the cylindrical pore. In that case we observe a high density of the square-well fluid in the center of the pore and a continuous, smooth, decrease to zero close to the wall $r \to R_{cyl}$. For $R_{cyl} \leq 5R_{HS}$, the liquid phase inside the pore is not stable and we find a gas phase at a low density. The gas packing fraction, which is indicated in the phase diagram in Fig. 1, is $\eta_g = 0.0378$ and follows from the equilibrium condition that the gas phase with this density has the same chemical potential as the high density liquid.

To ensure that the system undergoes a capillary evaporation transition and to locate the radius $R_{CE}$ at which it takes place, we also determine $\Omega[\rho(r)]/L$ the grand potential (per unit length) corresponding to the density profiles. We show the results as symbols in Fig. 3. There are several interesting features to appreciate. Obviously, there are two separate branches of the grand potential: one corresponding to the liquid phase for large values of $R_{cyl}$ and the other corresponding to the gas phase for small values of $R_{cyl}$. This, together with density profiles shown in Fig. 2 demonstrates that a capillary evaporation transition happens – it is not sufficient to look solely at the profiles. It is a strength of DFT that we are able to study both the profiles and the grand potentials at the same time and thereby elucidating the behavior of the system.

We can employ our DFT results, shown as symbols in Fig. 3, to verify the validity of the morphometric approach for the present problem. According to morphometry, the grand potential, Eq. (11), is quadratic in the radius of the cylinder. Using the thermodynamic coefficients $p_i$, $\sigma_i$ and $\kappa_i$ as fitting parameters, we fit Eq. (11) to our DFT data. The full and dashed line in Fig. 3 are the results of the fits to the grand potentials of the liquid and gas branch, respectively. The lines are in excellent agreement with the numerical data (symbols). The high quality of the fits demonstrate that the morphometric form of $\Omega$ can be employed, despite the fact that the pore is rather narrow, i.e. the pore size is sufficiently large compared to the correlation length $\xi$. This finding allows the conclusion that for the problem considered here, one can separate the thermodynamic coefficients from the geometry of the pore.

The thermodynamic coefficients as obtained by the fits are summarized in Tab. 1. The pressures $p_i$, $i = l, g$, are bulk properties and therefore can also be determined from the bulk equation of state. Both results for $p_i$ are in good agreement. Using these coefficients and Eq. (13) we obtain $R_{CE} = 5.73R_{HS}$ as the cylinder radius at which the transition takes place. This is in good agreement with the actual transition point. Given the high level of agreement between the morphometric form of $\Omega$ and the DFT results, this was to be expected.

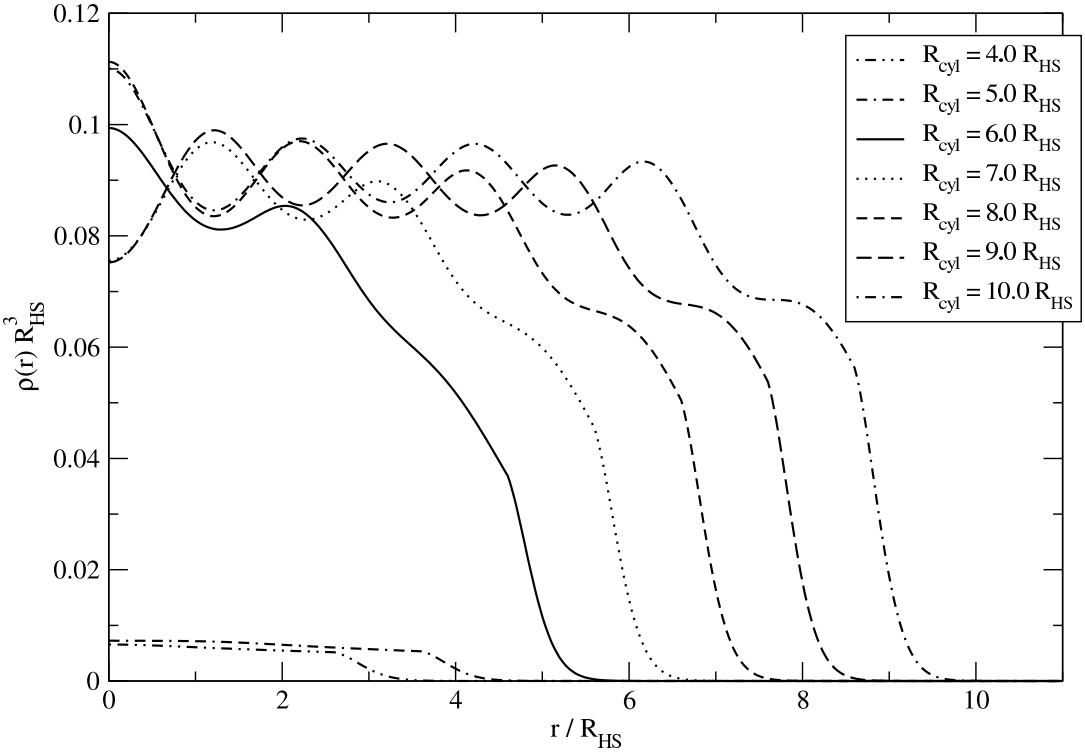


**Figure 2.** Density profiles $\rho(r)$ of a square well fluid inside of a cylindrical pore with hydrophobic wall-particle interaction as a function of the radius $R_{cyl}$. For radii $R_{cyl} \geq 6R_{HS}$ we find a liquid in the pore, while for $R_{cyl} \leq 5R_{HS}$ we find a gas. Note, however, that due to hysteresis effects it is not possible to determine the location of the capillary evaporation transition, which takes place at $R_{cyl} = R_{CE} \approx 5.73R_{HS}$, from the density profiles alone.

**Table 1.** Thermodynamic coefficients $p_i$, $\sigma_i$ and $\kappa_i$, $i = l, g$ obtained for a liquid and a gas inside a cylindrical pore from a fit to DFT results, assuming a morphometric form for the grand potential, Eq. (11).

| | liquid | gas |
|---|---|---|
| $\eta_i$ | 0.3842 | 0.0378 |
| $\beta p_i R_{HS}^3$ | $6.077 \times 10^{-2}$ | $5.507 \times 10^{-3}$ |
| $\beta \sigma_i R_{HS}^2$ | $2.066 \times 10^{-1}$ | $5.816 \times 10^{-3}$ |
| $\beta \kappa_i R_{HS}$ | $4.929 \times 10^{-1}$ | $7.708 \times 10^{-3}$ |

## 4. Capillary Evaporation in a Complex Geometry

For simple geometries, such as a slit pore, or an infinitely long cylindrical pore it is straightforward to perform DFT calculations in order to study the capillary evaporation phenomenon. It is also most instructive to study the thermodynamics and the density profiles at the same time. For more complex geometries a 'brute-force' [34] approach, in which density profiles are obtained by minimizing the DFT for the full geometry, is much more challenging. Therefore, in the following we will use only the morphometric approach to study the analog of capillary evaporation in a complex geometry. The geometrical model we

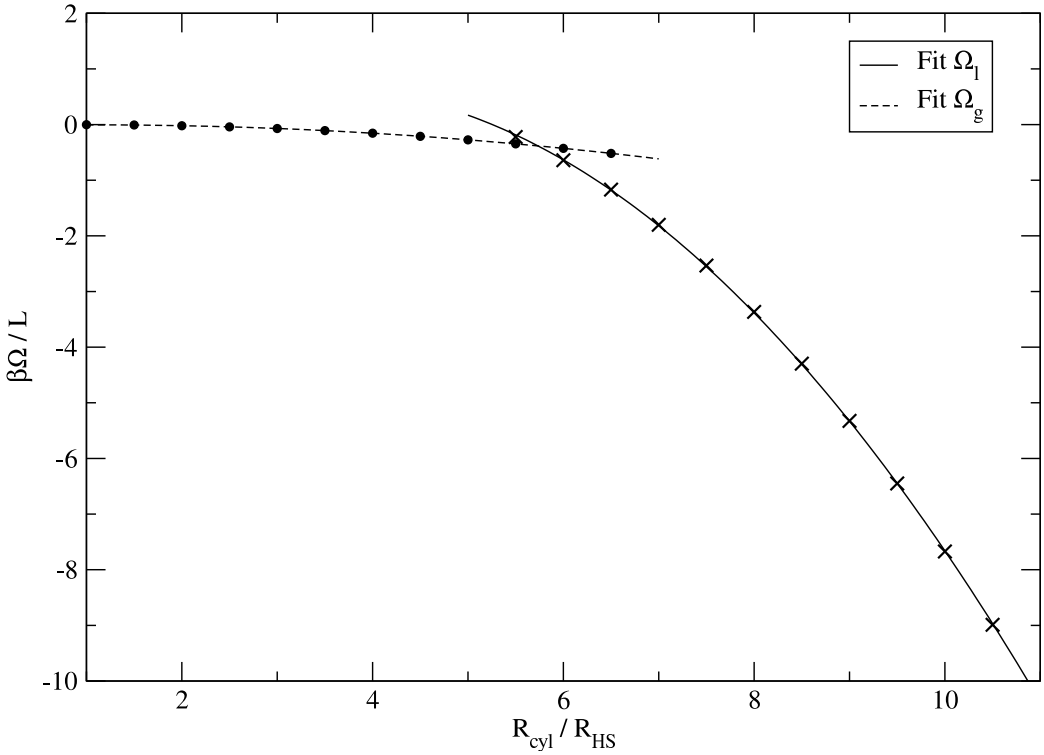


**Figure 3.** The grand potential per unit length of a square-well fluid inside an infinitely long cylindrical pore as function of the radius $R_{cyl}$. For large values of $R_{cyl}$ we find the liquid branch and for small values of $R_{cyl}$ the gas branch of the grand potential. Symbols correspond to DFT results and the full and dashed lines denote least-square fits according to the morphometric form, Eq. (11) of a fluid inside of a cylindrical pore. The agreement between the morphometric form and the numerical data is excellent, confirming the validity of morphometry in this situation.

wish to study is inspired by the structure of the voltage-gated potassium ion channels [35,36], shown in simplified model geometry in Fig. 4, which we approximate by a part of a cone. The parameters that prescribe the geometry are the radii $R_1$ and $R_2$ and the height $H$. In our model $R_1$ and $H$ are kept fixed and $R_2$ varies from a value large enough to stabilize the liquid in the gate, to a value small enough to allow for a closed gate with a gas bubble of height $h$ – see Fig. 4. We consider at both ends of the cone (or gate) to be big reservoirs of liquid, which will prevent the bubble from growing to macroscopic sizes. The bottom part of the gate connects to a spherical cavity of the potassium channel, while the top part of the gate connects to the inside of the cell. Due to the geometrical constraints, the bubble, if it forms, will always have a finite size and a finite number of liquid particles will be involved in the evaporation process. Hence, the formation of a bubble represents a pseudo phase transition. This implies that the state of the system constantly fluctuates between an open and a closed state and the probability of a transition is determined by the Boltzmann factor of the difference in grand potential between the states. In contrast to the capillary evaporation process in the infinitely long cylinder, which was either completely filled by the liquid or by the gas, we will observe two liquid-gas interfaces at the top and bottom ends of the bubble.

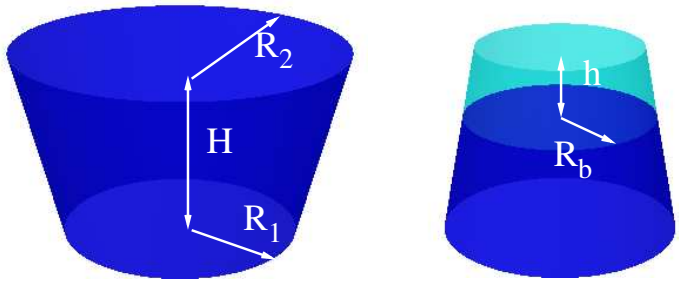


**Figure 4.** The model geometry of the gate of a potassium ion channel. The radius $R_1$ and the height $H$ are fixed and the radius $R_2$ is allowed to vary from a large value, for the open state of the gate, to a smaller one, for the closed state. In the open state, the whole gate is filled with liquid, while in the closed state, a gas bubble of height $h$ closes the gate and thereby stops the permeation of ions through the channel. $R_b$ is the radius of the bubble at the bottom. Note that in the closed state there are two liquid-gas interfaces at the top and bottom of the bubble.

In the following we consider the gate with a fixed configuration, i.e. with a given radius $R_2$, in a state in which it is entirely filled with the liquid and in a state with a bubble. By comparing these two states we examine the possibility of a bubble formation in the gate and study the behavior of the bubble, once it has formed. We employ the morphometric form of the grand potential for both a filled gate, which we denote as the open (op) state, and a gate with a gas bubble, which we denote as the closed (cl) state.

The grand potential of the open state is given by

$$\Omega^{op}_{gate}(R_2) = -p_l\, V(H, R_1, R_2) + \sigma_l\, M(H, R_1, R_2) + \kappa_l\, C(H, R_1, R_2), \quad (14)$$

with the thermodynamical coefficients $p_l$, $\sigma_l$ and $\kappa_l$ as specified in Tab. 1. The geometrical measures for a part of a cone with height $\tilde{h}$ and radii $r_1$ and $r_2$ at the bottom and the top, respectively, are specified by the volume

$$V(\tilde{h}, r_1, r_2) = \frac{\pi\tilde{h}}{3}\left(r_1^2 + r_2^2 + r_1 r_2\right), \quad (15)$$

the surface area of the cone shell

$$M(\tilde{h}, r_1, r_2) = \pi(r_1 + r_2)\sqrt{\tilde{h}^2 + (r_1 - r_2)^2}, \quad (16)$$

and the integrated (over the cone shell area) mean curvature

$$C(\tilde{h}, r_1, r_2) = -\pi\tilde{h}. \quad (17)$$

Like in the case of an infinitely long cylinder, the integrated (over the cone shell area) Gaussian curvature vanishes in the cone geometry, so that the grand potential of the liquid filled gate in the morphometric form, Eq. (14) is fully specified by three terms.

The morphometric form of a closed state of the gate, with a bubble of height $h$ is more complicated and contains terms for the part of the gate filled by the liquid, terms for the part filled by the gas, and terms due to presence of the liquid-gas interfaced. Assuming the simple

geometry shown in Fig. 4 we can write as ansatz

$$\begin{aligned}\Omega^{cl}_{gate}(h,R_2) = &-p_l\, V(H-h,R_1,R_b) + \sigma_l\, M(H-h,R_1,R_b) + \kappa_l\, C(H-h,R_1,R_b)\\ &-p_g\, V(h,R_b,R_2) + \sigma_g\, M(h,R_b,R_2) + \kappa_g\, C(h,R_b,R_2)\\ &+\sigma_{lg}\ (A(R_b)+A(R_2))\,. \end{aligned} \tag{18}$$

Note that by employing this ansatz we reduce the complexity of the problem of finding the state with lowest grand potential from a full DFT calculation in a complex geometry to a parametric minimization problem with a single free parameter, namely the bubble height $h$. The detailed shape of the bubble corresponding to the lowest grand potential will differ slightly from the shape assumed by this ansatz, however, we expect that *all* the essential physics is included in our approach. Furthermore, the simplicity of our approach allows us to gain deep insight into the driving factors of bubble formation and breaking in a gate-like geometry.

The radius $R_b$ in Eq. (18) depends on the geometrical parameters of the cone $R_1$, $R_2$, $H$ and the bubble height $h$ via $R_b = R_2 + h(R_1 - R_2)/H$. Clearly $R_2 < R_1$ is required to make this relation meaningful in the present context. Note that additional line-tension terms arise where the liquid-gas interface meets the wall. However, these contributions are expected to be small and should change the results, discussed below, only slightly. Therefore we neglect the line-tension terms in the following.

In order to fully specify the grand potential, Eq. (18), we require an additional thermodynamic coefficients namely $\sigma_{lg}$, the liquid-gas interface tension. Unfortunately, this quantity is rather difficult to calculate since we have to consider the interface between a liquid at high density and a gas phase, which is stabilized only in the confined geometry. This calculation could only be done in a brute-force application of DFT, which is prohibitive. Therefore we approximate the value of $\sigma_{lg}$ by the liquid-gas surface tension of the free interface between unconfined coexisting liquid and gas phases at the same temperature. This quantity can be calculated easily and we obtain $\beta\sigma_{lg}R^2_{HS} = 8.549 \times 10^{-2}$.

The surface area of the liquid-gas interface also calls for attention, since the radii $R_1$, $R_2$ and $R_b$ are measured at the dividing interface. The meaning of these radii becomes apparent when the density profiles in Fig. 2 are inspected carefully. For a radius of the cylindrical pore of e.g. $R_{cyl} = 10R_{HS}$, the liquid density profile drops to a vanishing density at $r \lesssim 9R_{HS}$. Therefore we use

$$A(r) = \pi(r - R_{HS})^2 \tag{19}$$

as the surface area of the liquid gas interface.

The first question to be addressed concerns the most probable bubble height $h_0$. This can be rephrased by asking which value of $h$ maximizes the difference in the grand potential between a closed and a open state of the gate, i.e.

$$\frac{\partial}{\partial h}\left(\Omega^{cl}_{gate}(h,R_2) - \Omega^{op}_{gate}(R_2)\right)\Big|_{h=h_0} = 0. \tag{20}$$

This equation can be solved explicitly. The result for $h_0(R_2)$, however, is quite lengthy and we therefore only show numerical results. With this result we can answer the question for

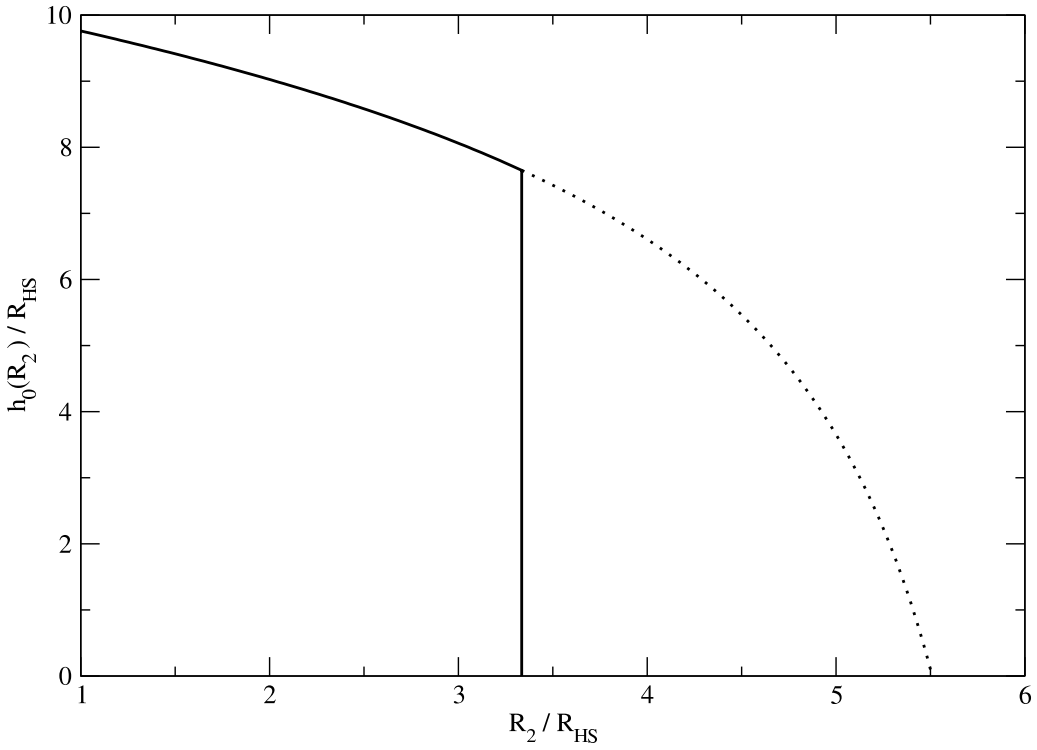


**Figure 5.** The most probable height $h_0(R_2)$ of the gas bubble as function of $R_2$. Due to the competition between the various contributions of the grand potential, the bubble height at the transition point at $R_2 = R_2^{max}$ is finite. For $R_2 < R_2^{max}$ a bubble with height $h_0(R_2)$ is the stable state, indicated by the full line, and the gate is closed. For $R_2 > R_2^{max}$, the closed gate is meta-stable, which is denoted by the dotted line – see Fig. 6.

which value of $R_2$ the stable state of the gate is the closed one. We denote the maximal value of $R_2$ for which a closed gate is stable with $R_2^{max}$, which is defined through

$$\Delta\Omega(R_2 = R_2^{max}) \equiv \Omega_{gate}^{cl}(h_0, R_2^{max}) - \Omega_{gate}^{op}(R_2^{max}) = 0, \tag{21}$$

which can be calculated numerically.

In order to quantify our results, we have to specify the geometry of the considered gate. We choose $R_1 = 7.14R_{HS}$ and $H = 12.86R_{HS}$, which corresponds to $R_1 \approx 10$Å and $H \approx 18$Å if we assign $R_{HS}$ a value of $1.4$Å as would be appropriate for water. For this choice of parameters, we plot in Fig. 5 the most probable height $h_0$ as a function of the parameter $R_2$. For large values of $R_2$, we find that a bubble of height $h_0(R_2)$ would be meta-stable, which we indicate by the dotted line. In this regime, the most stable state of the gate is the open state. As $R_2$ reaches the value of $R_2^{max}$, the bubble height jumps to a finite value and if $R_2$ is further decreased the bubble height increases slightly, as shown by the full line in Fig. 5. For the present model we find that the pseudo transition, at which a bubble forms in the gate, takes place for $R_2^{max} \approx 3.24R_{HS} \approx 4.53$Å , as follows from the difference in grand potential of a closed and open state of the gate as function of $R_2$ – see Fig. 6.

The finite height $h_0(R_2^{max})$ can be readily understood. When we compare the grand

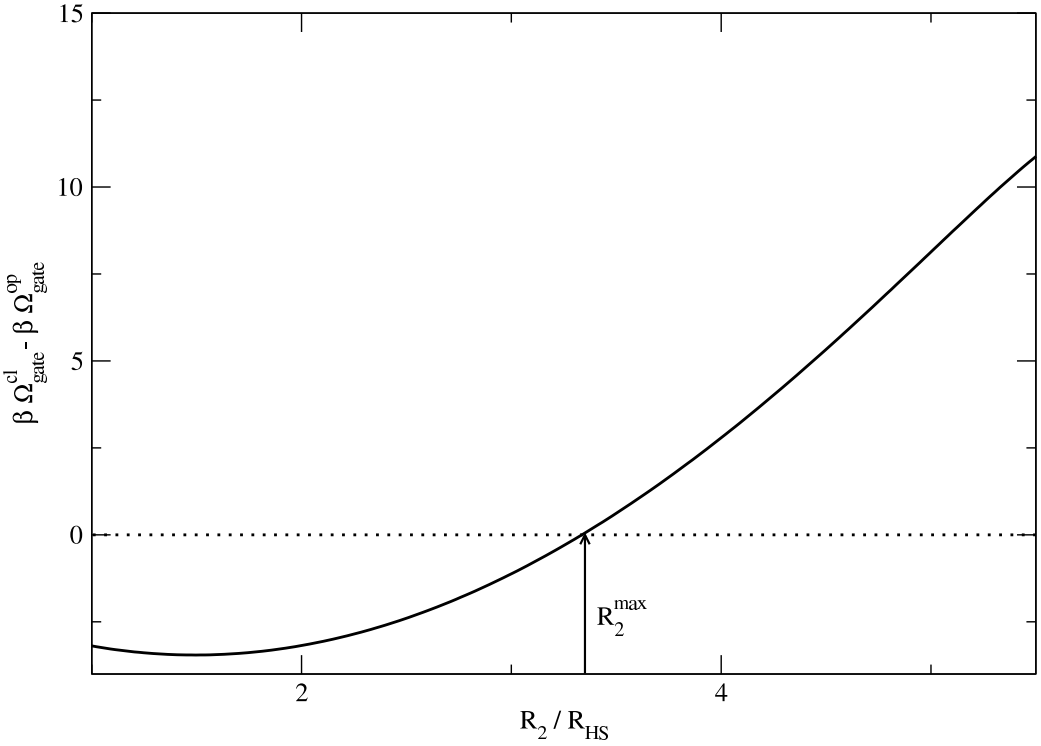


**Figure 6.** The difference in grand potential between a closed and an open state of the gate as function of $R_2$. If this difference is positive the open state is stable, otherwise, the closed state is stable. For $R_2 = R_2^{max}$ the difference in grand potential vanishes and thereby marks the transition point between the states of the gate.

potentials for the closed to that of the open state, by calculating $\Delta\Omega$ we find

$$\Delta\Omega(R_2) = -\Delta pV(h, R_b, R_2) + \Delta\sigma M(h, R_b, R_2) + \Delta\kappa C(h, R_b, R_2) + \sigma_{lg}\left(A(R_b) + A(R_2)\right), \tag{22}$$

where we have introduced $\Delta p = p_l - g_g$, $\Delta\sigma = \sigma_l - \sigma_g$ and $\Delta\kappa = \kappa_l - \kappa_g$. In order to have the gate closed we require $\Delta\Omega < 0$, which we can analyze by comparing the different contributions to $\Delta\Omega$. For the situation we consider here, we find that three terms in Eq. (22) are positive: $\Delta pV(h, R_b, R_2) > 0$, describing the fact that the volume term prefers the stable bulk phase, which is the liquid, in the gate, $\Delta\kappa C(h, R_b, R_2) > 0$, and $\sigma_{lg}(A(R_b) + A(R_2)) > 0$, which simple states the fact that the formation of two liquid-gas interfaces costs energy. These three contributions to $\Delta\Omega$ have to be balanced by the only negative term $\Delta\sigma M < 0$. However, this balance can only be established if the surface area of the cone shell $M$ is sufficiently large, which requires a finite height $h_0(R_2^{max})$.

Within this model of the gate, it is easy to estimate the energy required to *control* the state of the gate. If the gate is in the open state, then ion permeation should not be interrupted too often due to thermal fluctuations. This means that the value of $R_2$ in the open state has to be large enough that $\Delta\Omega$ stabilizes the open gate. However, if $R_2$ is too large in the open state, which would cause the gate to be constantly open, the energy cost to close the gate would be too high. Similar arguments can be employed for the closed state.

The closed state should also be stabilized against fluctuations, with sufficiently low energy costs. For our parameters, we can realize this situation if we assume that for the open state $R_2^{op} \approx R_2^{max} + 1.07R_{HS} \approx R_2^{max} + 1.5$Å and $R_2^{cl} \approx R_2^{max} - 1.42R_{HS} \approx R_2^{max} - 2$Å. In that case the energy required to control the gate is roughly $5k_BT$, which is comparable to the electrostatic energy gain of the voltage sensor of the potassium channel.

Finally we can estimate $\Delta N$ the number of liquid particles that leave the gate during a change in state in order to form the gas bubble. It is related to the difference between the liquid density $\rho_l$ and the gas density $\rho_g$ and the volume of the bubble

$$\Delta N(R_2) \approx (\rho_l - \rho_g)V(h, R_2 - R_{HS}, R_b - R_{HS}), \tag{23}$$

where the volume $V(h_0, R_2 - R_{HS}, R_b - R_{HS})$ is the volume accessible to the centers of fluid particles. For our system we plot the result in Fig. 7. The quantity $\Delta N$ specifies the most likely number of particles that leave the gate. From this estimate we conclude that roughly 14 to 19 liquid particles are involved in the transition between states. Since the bubble volume is rather small and the gas density low, one is unlikely to find an appreciable amount of particles inside the bubble. Note that a more accurate estimate can be obtained from the thermodynamic relation

$$\Delta\tilde{N}(R_2) = -\left(\frac{\partial\Omega_{gate}^{op}(R_2) - \Omega_{gate}^{cl}(h, R_2)}{\partial\mu}\right)\Bigg|_{T,V}. \tag{24}$$

The approximate expression, Eq. (23), takes only the volume term of the grand potentials into account and neglects the surface and curvature terms. In the present case the estimate, Eq. (23), is sufficient to describe the properties of the bubble.

## 5. Conclusion and Outlook

We have presented a model for the opening and closing of voltage-gated ion channel that follow the basic architecture of the KcsA channel. The hydrophobically lined gate region changes from a wide pore, when open, to a narrower pore when closed. We have shown with our morphometric approach to capillary evaporation in a hydrophobic pore with cone-shaped geometry that the formation of a bubble in the gate can close the permeation pathway of the channel and thereby stop the ion flux. For the morphometric approach we require a set of thermodynamic coefficients that we have determined in a simpler geometry within a set of DFT calculations for a square-well fluid. While the values of these coefficients differ significantly from the corresponding values for water, the fluid of biggest interest in the biological context of this model, a similar scenario should also be found in the case of water. It is the balance between different terms in the grand potential, i.e. the relative strength, rather than the absolute values of the thermodynamic coefficients that matter. Our model rationalizes recently seen bubble formation in computer simulations that employ more sophisticated models for water. We thereby provide a basis of understanding the role of bubble formation and breaking in the gating process of voltage-gated ion channels on a deeper level. Since this model identifies the important physical driving forces of the bubble formation, we hopefully provide a model that allows us to address, in addition to the basic (unperturbed)

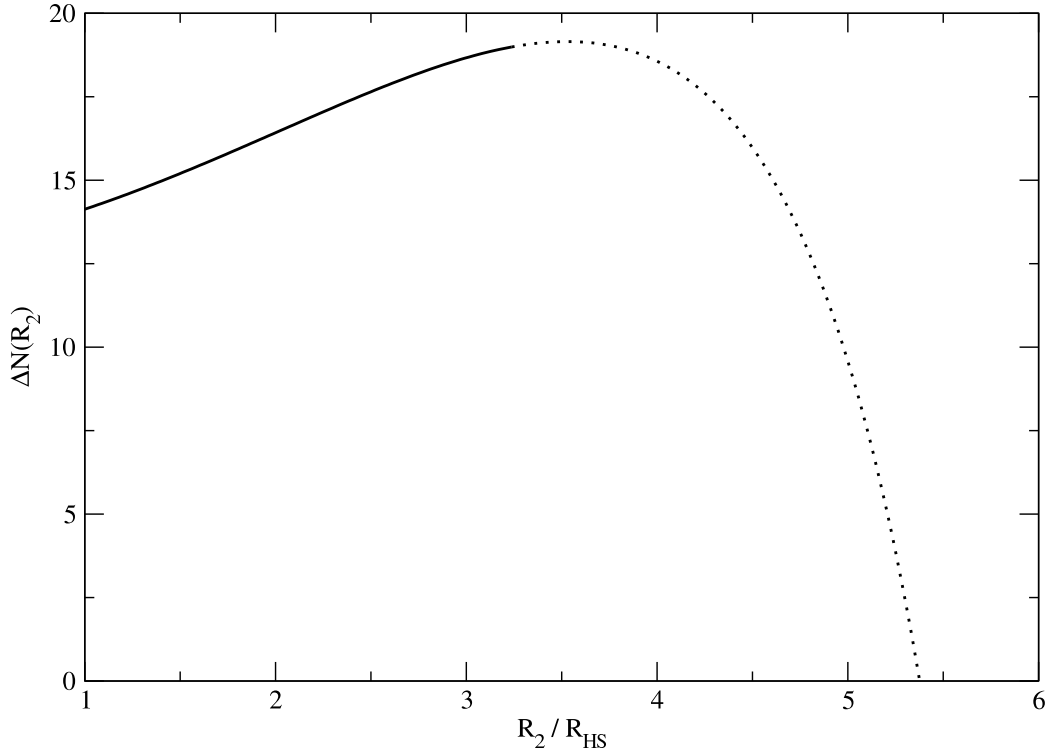


**Figure 7.** The number of fluid particles $\Delta N$ that leave the gate when a bubble forms to close the gate. If the gate is in the closed state, we plot $\Delta N$ as full line, when the gate is open we plot is as dotted line.

gating, other important properties of ion channels, such as the effect of various chemicals, that can change the environment in the gate, on the gating process.

In our study we have focused on the situation of changing geometry as a trigger for the bubble formation. However, it is easy to see within our description of a hydrophobic pore that a second mechanism for bubble formation can be identified from the balance between the surface term $\Delta\sigma M$ and all the other terms in Eq. (22): if the geometry is kept constant, $\Delta\Omega$ still can change sign and thereby favor the formation of a bubble if the degree of hydrophobicity and hence $\Delta\sigma$ is changed. This might be achieved if the gating process involves a change in charges in the gate as a way of controlling the protein-fluid interaction.

A combination of the geometrically controlled bubble formation, discussed in detail in this paper, and a chemically controlled bubble formation, mentioned above, is of course also possible and might be in use in mechanosensitive ion channels such as the tension activated MscS channel [22].

## Acknowledgments

RR is grateful to Wolfgang Nonner and Bob Eisenberg for many stimulating discussions about the role of bubble formation in the gating of ion channels and to Dirk Gillespie for comments on the manuscript.

## References


[1] Burgess CGV, Everett DH, and Nuttall S (1989) Pure Appl. Chem. **61** 1845.
[2] Wong APY and Chan MHW (1990) Phys. Rev. Lett. **65** 2567.
[3] Li JC, Ross DK, and Benham MJ (1991) J Appl. Cryst. **24** 794.
[4] Thommes M and Findenegg G H (1994) Langmuir **10** 4270.
[5] Thommes M, Findenegg G H and Schoen M (1995) Langmuir **11** 2137.
[6] Gross S and Findenegg G (1997) Ber. Bunsenges. Phys. Chem. **101** 1726.
[7] Morishige K and Shikimi M (1998) J. Chem. Phys. **108** 7821.
[8] Derjaguin B (1940) Acta Physicocgimica URSS **12** 181.
[9] Evans R, Marconi U B M, and Tarazona P (1986) J. Chem. Soc., Faraday Trans. 2 **86** 1763.
[10] Evans R (1986) J. Chem. Soc., Faraday Trans. 2 **82**, 1763.
[11] Evans R (1990) J. Phys.: Condens. Matter **2** 8989.
[12] Panagiotopoulos AZ (1987) Mol. Phys. **62** 701.
[13] Gregg SJ and Sing KSW (1967) in *Adsorption, Surface Area, and Porosity* (Academic Press: London)
[14] Spohr E, Trokhymchuk A, and Henderson D (1998) J. Electro. Chem. **450** 281.
[15] Noworyta J P, Henderson D, and Sokołowski S (1999) Mol. Phys. **96** 1139.
[16] Allen R, Melchionna S, and Hansen JP (2002) Phys. Rev. Lett. **89** 175502.
[17] Allen R, Hansen JP, and Melchionna S (2003) J. Chem. Phys. **119** 3905.
[18] Dzubiella J and Hansen JP (2005) J. Chem. Phys. 234706.
[19] Beckstein O, Biggin PC, Sansom MSP (2001) J. Phys. Chem. B **105** 12902.
[20] Beckstein O and Sansom MSP (2003) Proc. Natl. Acad. Sci. U.S.A. **100** 7063.
[21] Beckstein O and Sansom MSP (2004) Phys. Biol. **1** 42.
[22] Anishkin A and Sukharev S (2004) Biophys. J. **86** 2883.
[23] Sriraman S, Kevrekidis IG, and Hummer G (2005) Phys. Rev. Lett. **95** 130603.
[24] Hille B (2001) in *Ion Channels of Exciteable Membranes*, (Sinauer Asc.: Sunderland).
[25] see, e.g. Evans R 1992 in *Fundamentals of Inhomogeneous Fluids* (New York: Dekker) p 85
[26] König P M, Roth R, and Mecke K R 2004 Phys. Rev. Lett. **93** 160601
[27] Roth R 2005 J. Phys.:Condens. Matter **17** S3463
[28] Roth R, Evans R, Lang A, and Kahl G 2002 J. Phys.:Condens. Matter **14** 12063
[29] Yu Y-X and Wu J 2002 J. Chem. Phys. **117** 10156
[30] Rosenfeld Y 1989 Phys. Rev. Lett. **63** 980.
[31] Sullivan DE, Levesque D, and Weiss JJ (1980) J. Chem. Phys. **72** 1170.
[32] Bryk P, Roth R, Mecke KR, and Dietrich S (2003) Phys. Rev. E **68** 031602.
[33] Roth R and Gillespie D 2005 Phys. Rev. Lett. **95** 247801.
[34] Ustinow EA and Do DD (2005) Adsorption **11** 455.
[35] Doyle DA et al. (1998) Science **280** 69.
[36] Jiang Y et al. (2002) Nature **417** 515.